

1 **Title:** Six new reference-quality bat genomes illuminate the molecular basis and evolution of
2 bat adaptations

3
4 **Authors:** David Jebb^{1,2,3}, Zixia Huang ⁴ Martin Pippel^{1,3}, Graham M. Hughes⁴, Ksenia
5 Lavrichenko⁵, Paolo Devanna⁵, Sylke Winkler¹, Lars S. Jermini^{4,6,7}, Emilia C. Skirmuntt⁸, Aris
6 Katzourakis⁸, Lucy Burkitt-Gray⁹, David A. Ray¹⁰, Kevin A. M. Sullivan¹⁰, Juliana G.
7 Roscito^{1,2,3}, Bogdan M. Kirilenko^{1,2,3}, Liliana M. Dávalos^{11,12}, Angelique P. Corthals¹³, Megan
8 L. Power⁴, Gareth Jones¹⁴, Roger D. Ransome¹⁴, Dina Dechmann^{15,16,17}, Andrea G.
9 Locatelli⁴, Sébastien J. Puechmaille^{18,19}, Olivier Fedrigo²⁰, Erich D. Jarvis^{21,22}, Mark S.
10 Springer²³, Michael Hiller^{*1,2,3}, Sonja C. Vernes^{*5,24}, Eugene W. Myers^{*1,3,25}, Emma C.
11 Teeling^{*4}

12
13 ¹Max Planck Institute of Molecular Cell Biology and Genetics, Dresden, Germany

14 ²Max Planck Institute for the Physics of Complex Systems, Dresden, Germany

15 ³Center for Systems Biology Dresden, Dresden, Germany

16 ⁴School of Biology and Environmental Science, University College Dublin, Dublin, Ireland

17 ⁵Neurogenetics of Vocal Communication Group, Max Planck Institute for Psycholinguistics,
18 Nijmegen, The Netherlands

19 ⁶Research School of Biology, Australian National University, Canberra, ACT, Australia

20 ⁷Earth Institute, University College Dublin, Dublin, Ireland

21 ⁸Peter Medawar Building for Pathogen Research, Department of Zoology, University of Oxford,
22 Oxford, United Kingdom

23 ⁹Conway Institute of Biomolecular and Biomedical Science, University College Dublin, Dublin,
24 Ireland

25 ¹⁰Department of Biological Sciences, Texas Tech University, Lubbock, USA

26 ¹¹Department of Ecology and Evolution, Stony Brook University, Stony Brook, Stony Brook, USA

27 ¹²Consortium for Inter Disciplinary Environmental Research, Stony Brook University, Stony Brook,
28 USA

29 ¹³Department of Sciences, John Jay College of Criminal Justice, New York, USA

30 ¹⁴School of Biological Sciences, University of Bristol, Bristol, United Kingdom

31 ¹⁵Department of Migration and Immuno-Ecology, Max Planck Institute of Animal Behavior,
32 Radolfzell, Germany

33 ¹⁶Department of Biology, University of Konstanz, Konstanz, Germany

34 ¹⁷Smithsonian Tropical Research Institute; Panama City, Panama

35 ¹⁸ISEM, University of Montpellier, Montpellier, France

36 ¹⁹Zoological Institute and Museum, University of Greifswald, Greifswald, Germany

37 ²⁰Vertebrate Genomes Laboratory, The Rockefeller University, New York, NY, USA

38 ²¹Laboratory of Neurogenetics of Language, The Rockefeller University, New York, NY, USA

39 ²²Howard Hughes Medical Institute, Chevy Chase, MD, USA

40 ²³Department of Biology, University of California, Riverside, CA, USA

41 ²⁴Donders Institute for Brain, Cognition and Behaviour, Nijmegen, The Netherlands

42 ²⁵Faculty of Computer Science, Technical University Dresden, Dresden, Germany

43

44 ^{*}Joint first authors

45 ^{*}joint senior/corresponding authors emails

46 Michael Hiller: hiller@mpi-cbg.de

47 Sonja Vernes: sonja.vernes@mpi.nl

48 Eugene Myers: gene@mpi-cbg.de

49 Emma C. Teeling: emma.teeling@ucd.ie

50 **Abstract:** Bats account for ~20% of all extant mammal species and are considered exceptional
51 given their extraordinary adaptations, including biosonar, true flight, extreme longevity, and
52 unparalleled immune systems. To understand these adaptations, we generated reference-quality
53 genomes of six species representing the key divergent lineages. We assembled these genomes
54 with a novel pipeline incorporating state-of-the-art long-read and long-range sequencing and
55 assembly techniques. The genomes were annotated using a maximal evidence approach, *de*
56 *novo* predictions, protein/mRNA alignments, Iso-seq long read and RNA-seq short read
57 transcripts, and gene projections from our new TOGA pipeline, retrieving virtually all (>99%)
58 mammalian BUSCO genes. Phylogenetic analyses of 12,931 protein coding-genes and 10,857
59 conserved non-coding elements identified across 48 mammalian genomes helped to resolve
60 bats' closest extant relatives within Laurasiatheria, supporting a basal position for bats within
61 Scrotifera. Genome-wide screens along the bat ancestral branch revealed (a) selection on
62 hearing-involved genes (e.g. *LRP2*, *SERPINB6*, *TJP2*), which suggest that laryngeal
63 echolocation is a shared ancestral trait of bats; (b) selection (e.g. *INAVA*, *CXCL13*, *NPSR1*) and
64 loss of immunity related proteins (e.g. *LRRC70*, *IL36G*), including pro-inflammatory NF- κ B
65 signalling; and (c) expansion of the *APOBEC* family, associated with restricting viral infection,
66 transposon activity and interferon signalling. We also identified unique integrated viruses,
67 indicating that bats have a history of tolerating viral pathogens, lethal to other mammal species.
68 Non-coding RNA analyses identified variant and novel microRNAs, revealing regulatory
69 relationships that may contribute to phenotypic diversity in bats. Together, our reference-
70 quality genomes, high-quality annotations, genome-wide screens and *in-vitro* tests revealed
71 previously unknown genomic adaptations in bats that may explain their extraordinary traits.

72

73 **Keywords:** Bats, genomes, immunity, flight, ageing, miRNA, viruses, longevity, echolocation

74 **Introduction.**

75 With more than ~1400 species identified to date¹, bats (Chiroptera) account for ~20% of all
76 currently recognised, extant, mammal species, are found around the globe, and successfully
77 occupy diverse ecological niches^{1,2}. Their global success is attributed to their extraordinary
78 suite of adaptations including: powered flight, laryngeal echolocation for orientation and
79 hunting in complete darkness, exceptional longevity, and a unique immune system that enables
80 bats to tolerate viruses that are typically lethal in other mammals (e.g., rabies, SARS, MERS)².
81 It has been proposed that the evolution of extended longevity and immunity in bats was driven
82 by the acquisition of flight, which has a high metabolic cost³⁻⁵, but the mechanisms underlying
83 these adaptations are unknown and their potential connection to flight is still debated^{6,7}. Given
84 bats' distinctive adaptations, they represent important model systems to uncover the molecular
85 basis and evolution of extended healthspan^{7,8}, enhanced disease tolerance⁹ and sensory
86 perception^{10,11}. To understand the evolution of such traits, one needs to understand bats'
87 evolutionary history. However, key aspects of that evolutionary history such as monophyly of
88 echolocating bats and the single origin of laryngeal echolocation^{10,12} remain debated, partially
89 stemming from a poor fossil record¹³, incongruent phylogenetic analyses¹⁴, and importantly the
90 limited quality of available genome assemblies.

91

92 Here, we generated the first reference-quality genomes of six bats as part of the Bat1K global
93 genome consortium² (<http://bat1k.com>) in coordination with the Vertebrate Genome Project
94 (<https://vertebratogenomesproject.org/>). Species were chosen to enable capture of the major
95 ecological trait space and life histories observed in bats while representing deep phylogenetic
96 divergences. These six bat species belong to five families that represent key evolutionary
97 clades, unique adaptations and span both major lineages in Chiroptera estimated to have
98 diverged ~64 MYA¹⁵. In the suborder Yinpterochiroptera we sequenced *Rhinolophus*
99 *ferrumequinum* (Greater horseshoe bat; family Rhinolophidae) and *Rousettus aegyptiacus*
100 (Egyptian fruit bat; Pteropodidae), and in Yangochiroptera we sequenced *Phyllostomus*
101 *discolor* (Pale spear-nose bat; Phyllostomidae), *Myotis myotis* (Greater mouse-eared bat;
102 Vespertilionidae), *Pipistrellus kuhlii* (Kuhl's pipistrelle; Vespertilionidae) and *Molossus*
103 *molossus* (Velvety free-tailed bat; Molossidae) (Table S1). These bat genera represent the
104 extremes in known bat longevity¹⁶. They also represent major adaptations in bat sensory
105 perception and ecological diversity², and include species considered key viral reservoirs and
106 asymptomatic hosts^{9,17}.

107

108 To obtain genome assemblies of high contiguity and completeness, we developed novel
109 pipelines incorporating state-of-the-art sequencing and assembly. To ascertain the position of
110 Chiroptera within Laurasiatheria and thus resolve a long-standing phylogenetic debate¹⁴, we
111 mined these near complete genomes to produce a comprehensive orthologous gene data set
112 (12,931), including data from 42 other representative mammalian genomes (TableS1), and
113 applied a suite of diverse phylogenetic approaches. To identify molecular changes in regions
114 of the genome - both coding and non-coding - that underlie bat adaptations, we carried out
115 selection tests, analysed gains and losses of genes, and experimentally validated novel bat
116 microRNAs. We focussed on assessing the shared commonalities between the bat species
117 enabling us to infer the ancestral selection driving key bat adaptations. We elucidated the
118 diversity of endogenous viruses contained within the bat genomes, exploring bats' putative
119 history with these viruses. Herein, we present the first six reference-quality bat genomes, which
120 we make available in the open access Bat1K browser (also available on NCBI and GenomeArk)
121 and demonstrate both the value of highly contiguous and highly complete genomes and the
122 utility of bats as model organisms to address fundamental questions in biology.

123

124 **Genome Sequencing and Assembly**

125 For each of the six bats, we generated: (i) PacBio long reads (52-70X in reads \geq 4 kb; N50 read
126 length 14.9-24.5 kb), (ii) 10x Genomics Illumina read clouds (43-104X), (iii) Bionano optical
127 maps (coverage of molecules \geq 150 kb 89-288X), and (iv) Hi-C Illumina read pairs (15-95X).
128 PacBio reads were assembled into contigs with a customized assembler called DAmar, a hybrid
129 of our earlier Marvel¹⁸, Dazzler (<https://dazzlerblog.wordpress.com/>), and Daccord^{19,20} systems
130 (Fig. 1a). Next, we used PacBio reads and 10x read cloud Illumina data to remove base errors,
131 which was followed by identifying and phasing all regions of the contigs that had a sufficient
132 rate of haplotype heterogeneity. We retained one haplotype for each region, yielding primary
133 contigs. These primary contigs were then scaffolded using a Bionano optical map and the Hi-C
134 data (see supplementary methods section 2).

135

136 For all six bats, this sequencing and assembly strategy produced assemblies with contig N50
137 values ranging from 10.6 to 22.2 Mb (Fig. 1b, Table S2). Thus, our contigs are \geq 355 times
138 more contiguous than the recent *Miniopterus* assembly generated from short read data²¹, and
139 \geq 7 times more contiguous than a previous *Rousettus* assembly generated from a hybrid of short
140 and long read data²² (Fig. 1b). Our scaffold N50 values ranged from 80.2 to 171.1 Mb and were
141 often limited by the size of chromosomes (Fig. 1b, Table S2). We estimated that 87 to 99% of

142 each assembly is in chromosome-level scaffolds (Table S3). Consensus base accuracies across
143 the entire assembly range from QV 40.8 to 46.2 (Table S2) for the six bats (where QV 40
144 represents 1 error in 10,000 bp). Since the algorithms for assembling, scaffolding, and
145 haplotyping are an active area of research²³, we expect that in the future even more complete
146 genome reconstructions can be produced with the data we collected. Even so, our current
147 strategy and algorithms generated chromosome-level assemblies of the six bats with
148 unprecedented contiguity, which are comparable to the best reference-quality genomes
149 currently generated for any eukaryotic species with a complex, multi-gigabyte genome²⁴.
150 Importantly, they meet the Vertebrate Genome Project (VGP) minimum standard of 3.4.2QV40
151 and have been added to the VGP collection.

152
153 To assess genome completeness, we first evaluated the presence of 4,104 genes that are highly
154 conserved among mammals (BUSCO, Benchmarking Universal Single-Copy Orthologs²⁵).
155 Between 92.9 and 95.8% of these genes were completely present in our assemblies, which is
156 comparable to the assemblies of human, mouse, and other Laurasiatheria (Fig. 1c, Table S4).
157 Second, to assess completeness in non-exonic genomic regions, we determined how many of
158 197 non-exonic ultraconserved elements (UCEs)²⁶ align at $\geq 85\%$ identity to the human
159 sequence. As expected, the vast majority of UCEs were detected in all assemblies (Fig. 1d).
160 Two to four UCEs were not detected in *Miniopterus*, dog, cat, and cow due to assembly
161 incompleteness (i.e. assembly gaps; Table S5, Fig. S1). In the bat genomes reported herein, no
162 UCEs were missing due to assembly incompleteness. Instead, one to three UCEs were not
163 detected in our *Myotis* and *Pipistrellus* assemblies because the UCE sequences are more than
164 85% diverged (Table S5), a striking result given that UCE's are highly conserved across other
165 more divergent mammals (e.g. human-mouse-rat comparison). To determine if this sequence
166 divergence was caused by base errors in the assemblies, we aligned raw PacBio and Illumina
167 reads and sequencing data of related bats, which confirmed that these UCEs are truly diverged
168 (Figs. S1-S5). In summary, our six bat assemblies are highly complete and revealed the first
169 examples of highly diverged UCEs.

170
171 **Genome Annotation**
172 To comprehensively annotate genes, we integrated a variety of evidence (Fig. 1e). First, we
173 aligned protein and cDNA sequences of a related bat species to each of our six genomes (Table
174 S6). Second, we projected genes annotated in human, mouse²⁷ and two bat assemblies (*Myotis*
175 *lucifugus* (Ensembl) and *Myotis myotis* (Bat1K)) to our genomes via whole-genome

176 alignments²⁸. Third, we generated *de novo* gene predictions by applying Augustus²⁹ with a
177 trained bat-specific gene model in single-genome mode to individual genomes, and in
178 comparative mode to a multiple genome alignment including our bat assemblies. Fourth, we
179 integrated transcriptomic data from both publicly available data sources and our own Illumina
180 short read RNA-seq data (Table S7). Additionally, we generated PacBio long read RNA
181 sequences (Iso-seq) from all six species to capture full-length isoforms and accurately annotate
182 untranslated regions (UTRs) (Table S8). Iso-seq data were processed using the TAMA
183 pipeline³⁰ which allowed capturing a substantially greater diversity of transcripts and isoforms
184 than the default pipeline (<https://github.com/PacificBiosciences/IsoSeq3>). All transcriptomic,
185 homology-based and *ab initio* evidence were integrated into a consensus gene annotation that
186 we further enriched for high-confidence transcript variants and filtered for strong coding
187 potential.

188

189 For the six bats, we annotated between 19,122 and 21,303 coding genes (Fig. 1f). These
190 annotations completely contain between 99.3 and 99.7% of the 4,104 highly conserved
191 mammalian BUSCO genes (Fig. 1f, Table S4), showing that our six bat assemblies are highly
192 complete in coding sequences. Since every annotated gene is by definition present in the
193 assembly, one would expect that BUSCO applied to the protein sequences of annotated genes
194 and BUSCO applied to the genome assembly should yield highly similar statistics. However,
195 the latter finds only 92.9 to 95.8% of the exact same gene set as completely present, showing
196 that BUSCO applied to an assembly only, underestimates the number of completely contained
197 genes. Importantly, this gene annotation completeness of our bats is higher than the Ensembl
198 gene annotations of dog, cat, horse, cow and pig, and is only surpassed by the gene annotations
199 of human and mouse, which have received extensive manual curation of gene models (Fig. 1f,
200 Table S4). This suggests reference-quality genome assemblies and the integration of various
201 gene evidence as detailed above, can be used to generate high-quality and near-complete gene
202 annotations of bats as well as other species too. All individual evidence and the final gene set
203 can be visualized and obtained from the Bat1K genome browser (<https://genome-public.pks.mpg.de>).

205

206 **Genome Sizes and Transposable Elements**

207 At ~2 Gb, bat genomes are generally smaller than genomes of other placental mammals that
208 are typically between 2.5 and 3.5 Gb². Nevertheless, our assemblies revealed noticeable
209 genome size differences within bats, with assembly sizes ranging from 1.78 Gb for *Pipistrellus*

210 to 2.32 Gb for *Molossus* (Fig. 1g). As genome size is often correlated with transposable element
211 (TE) content and activity, we focused on the genomes of the six bats and seven other
212 representative Boreoeutherian mammals (Laurasiatheria + Euarchontoglires), selected for the
213 highest genome contiguity, and used a previously-described workflow and manual curation to
214 annotate TEs³¹. This showed that TE content generally correlates with genome size (Fig. 1g).
215 Next, we compared TE copies to their consensus sequence to obtain a relative age from each
216 TE family. This revealed an extremely variable repertoire of TE families with evidence of
217 recent accumulation (defined as consisting of insertions with divergences<6.6% from the
218 relevant consensus sequence). For example, while the 1.89 Gb *Rousettus* genome exhibits few
219 recent TE accumulations, ~0.38%, while ~4.2% of the similarly sized 1.78 Gb *Pipistrellus*
220 genome is derived from recent TE insertions (Fig. 1g-h). The types of TE that underwent recent
221 expansions also differ substantially in bats compared to other mammals, particularly in regards
222 to the evidence of recent accumulation by rolling-circle and DNA transposons in the
223 vespertilionid bats (Fig. 1g-h). These two TE classes have been largely dormant in most
224 mammals for the past ~40 million years and recent insertions are essentially absent from other
225 Boreoeutherian genomes³². These results add to previous findings revealing a substantial
226 diversity in TE content within bats, with some species exhibiting recent and ongoing
227 accumulation from TE classes that are extinct in most other mammals while other species show
228 negligible evidence of TE activity³³.

229

230 **The Origin of Chiroptera within Laurasiatheria**

231 Identifying the evolutionary origin of bats within Laurasiatheria is a key prerequisite for
232 comparative analyses aimed at revealing the genomic basis of traits shared by bats. However,
233 the phylogeny of Laurasiatheria and, in particular, the position of bats has been a long-standing,
234 unresolved phylogenetic question^{14,34}. This is perhaps the most challenging interordinal
235 problem in placental mammal phylogenetics, as multiple phylogenetic and systematic
236 investigations using large nucleotide and genomic scale datasets or transposable element
237 insertions support alternative topologies³⁵. These incongruent results have been attributed to
238 the challenge of identifying two, presumably short, internal branches linking four clades
239 (Chiroptera, Cetartiodactyla, Perissodactyla, Carnivora + Pholidota) that diverged in the Late
240 Cretaceous³⁵.

241

242 We revisited this question leveraging the high completeness of our gene annotation. First, we
243 extracted a comprehensive set of 12,931 orthologous protein-coding genes from the 48

244 mammalian genomes, resulting in a dataset comprising 21,471,921 aligned nucleotides in
245 length, which contained 7,913,054 parsimony-informative sites. The best-fit model of sequence
246 evolution for each of the 12,931 gene alignments was inferred using ModelFinder³⁶ (Table S9).
247 The species tree was then estimated by maximum likelihood using the model-partitioned
248 dataset with IQTREE³⁷ and rooted on Atlantogenata³⁸. Branch-support values were obtained
249 by UFBoot³⁹ with 1000 bootstrap pseudoreplicates. These analyses led to 100% bootstrap
250 support across the entire tree (Fig. 2a) and seemingly identified the origin of bats within
251 Laurasiatheria. The basal split is between Eulipotyphla and other laurasiatherians (i.e.,
252 Scrotifera). Within Scrotifera, Chiroptera is the sister clade to Fereuungulata (Cetartiodactyla
253 + Perissodactyla + Carnivora + Pholidota). This tree disagrees with the Pegasoferae
254 hypothesis⁴⁰, which groups bats with Perissodactyla, Carnivora and Pholidota, but agrees with
255 concatenation analyses of phylogenomic data⁴¹. Evolutionary studies based on 102
256 retroposons, including ILS-aware analyses, also support a sister-group relationship between
257 Chiroptera and Fereuungulata, but differ from the present analyses in supporting a sister-group
258 relationship between Carnivora and Cetartiodactyla^{34,35}. However, as the number of
259 homologous sites increases in phylogenomic datasets, so too does bootstrap support⁴², even
260 sometimes for an incorrect phylogeny⁴³, and as non-coding sequences can produce a different
261 topology than coding sequences⁴⁴, we further explored the phylogenomic signal within our
262 genomes.

263
264 To assess whether the tree inferred from the concatenated dataset (Fig. 2a) is also supported by
265 the non-coding part of the genome, we estimated a phylogeny using the models of best fit
266 (Table S9) for a dataset comprising 10,857 orthologous conserved non-coding elements
267 (CNEs), which contained 5,234,049 nucleotides and 1,225,098 parsimony-informative sites
268 (Table S10), using methods as described above. The result of this analysis (Fig. 2b) supports a
269 tree similar but not identical to that inferred from the protein-coding sequences (Fig. 2a),
270 including a sister-group relationship between Chiroptera and Fereuungulata, but with
271 Perissodactyla more closely related to Carnivora + Pholidota than to Cetartiodactyla. The CNE
272 tree also recovered a different position for *Tupaia* (Scandentia) within Euarchontoglires.

273
274 Given that two very short branches at the base of Scrotifera define relationships between its
275 four major clades (Carnivora + Pholidota, Cetartiodactyla, Chiroptera, Perissodactyla), this
276 region of the placental tree may be in the “anomaly zone”, defined as a region of tree space
277 where the most common gene tree(s) differs from the species tree topology⁴⁵. In the case of

278 four taxa and a rooted pectinate species tree, anomalous gene trees should be symmetric rather
279 than pectinate. To explore this, we estimated the maximum-likelihood support of each protein-
280 coding gene (n=12,931) for the 15 possible bifurcating topologies involving four clades, in our
281 case with Eulipotyphla as the outgroup (Fig. S6), and with the sub-trees for the relevant clades
282 identical to those in Fig. 2a. Based on the log-likelihood scores, 2,104 gene alignments
283 supported more than one tree, so these genes were excluded from further analysis. The
284 remaining 10,827 genes supported one fixed tree topology over the other 14 (Table S11), with
285 the number of genes supporting each topology highlighted in Fig. 2c. The best-supported
286 topology was that of our concatenated dataset for protein-coding genes (Fig. 2a; Tree1 with
287 1007/10827 genes), showing a sister group relationship between Chiroptera and Fereuungulata,
288 which is also supported by the CNEs (Fig. 2b). This suggests that the majority of the genome
289 supports a sister relationship between Chiroptera and the other Scrotifera. That said, there were
290 four other topologies that had support from >800 genes (Tree14 883/10827; Tree04 865/10827;
291 Tree15 820/10827; Tree13 806/10827) (Fig. 2c). However, even with similar support levels
292 for several topologies, the phylogenetic position for Chiroptera is pectinate on the most
293 common gene tree and does not qualify as anomalous. If the base of Scrotifera is in the anomaly
294 zone, as suggested by coalescence analyses of retroposon insertions³⁵, then we may expect the
295 most common gene tree(s) to be symmetric rather than pectinate. We may also expect the
296 species tree based on concatenation to be symmetric instead of pectinate⁴⁵. One explanation for
297 the absence of anomalous gene trees, and for a pectinate species tree based on concatenation,
298 is that both protein-coding genes and CNEs are generally under purifying selection, which
299 reduces both coalescence times and incomplete lineage sorting relative to neutrally evolving
300 loci^{46,47}.

301
302 Bias in phylogenetic estimates can also be due to model misspecification, which is an
303 inadequate fit between phylogenetic data and the model of sequence evolution used⁴⁸.
304 Misleading support for incorrect phylogenies can also be due to gene tree error arising from a
305 lack of phylogenetic informativeness amongst data partitions⁴⁹. To overcome these biases, we
306 performed a series of compatibility analyses on each gene partition and across the supermatrix
307 at 1st, 2nd and 3rd codon sites; 1st + 2nd codon sites; 1st + 2nd + 3rd codon sites; amino acids,
308 assuming a 4-state alphabet for nucleotides and a 20 state-alphabet for amino acids (see
309 supplementary methods section 4.2). We excluded all alignments for which evidence of
310 saturation of substitutions and thus decay of the historical signal was detected by SatuRation
311 1.0 (<https://github.com/lsjermiin/SatuRationSatuRation>). Furthermore, we excluded all

312 alignments for which model mis-specification due to evolution under non-homogeneous
313 conditions was detected by the matched-pairs test of symmetry⁵⁰ implemented in Homo 2.0
314 (<https://github.com/lsjermiin/Homo2.0>).

315
316 A total of 488 gene alignments, consisting of 1st and 2nd codon positions and containing all
317 48 taxa, were considered optimal for phylogenetic analysis (Table S12). We concatenated these
318 data into a supermatrix of 241,098 nucleotides in length with 37,588 informative positions and
319 completed all phylogenetic analyses using methods as described above. However, this reduced
320 data set did not provide an unambiguous phylogenetic estimate. Specifically, while the best-
321 supported topology differed from the best trees inferred using all protein-coding genes and
322 CNEs in its position of Chiroptera, which is now sister to Carnivora + Pholidota (Fig. 2d), this
323 node has low bootstrap support (58%; topology 13; Fig. 2d) and Approximately Unbiased (AU)
324 tests could not reject the topologies depicted in Fig. 2a and 2b. Furthermore, the phylogeny
325 inferred from the subset of 488 genes is also symmetric for the four major lineages of
326 Scrotifera, as may be expected if this node is in the anomaly zone and concatenation is
327 misleading. We further analysed these data using a single-site coalescence-based method,
328 SVDquartets^{51,52}, which provides an alternative to concatenation. The resulting optimal
329 topology also supported Chiroptera as sister taxa to Fereuungulata (Fig. S7, topology 1), which
330 is the most supported position from all of our analyses and data partitions.

331
332 Taken together, multiple lines of evidence suggest that the majority of the genome supports
333 Chiroptera as sister to all other scrotiferans. However, different regions of the genome can and
334 do reflect alternative evolutionary scenarios. This highlights the importance of generating
335 phylogenetic inferences from multiple genomic regions and the importance of screening these
336 regions for violations of phylogenetic assumptions and incongruent signals, especially when
337 dealing with short internal branches.

338
339 **Genome-wide screens for gene selection, losses and gains**
340 To study the genomic basis of exceptional traits shared by bats, we first performed three
341 unbiased genome-wide screens for gene changes that occurred in the six bats. First, we
342 screened 12,931 genes classified as 1:1 orthologs for signatures of positive selection on the
343 ancestral bat (stem Chiroptera) branch under the aBSREL model⁵³ using HyPhy⁵⁴ and the
344 best-supported phylogeny (Fig. 2a). For genes with significant evidence for selection after
345 multiple test correction (FDR<0.05), we manually inspected the underlying alignment to

346 ensure homology (supplementary methods section 4.3.1), and additionally required that the
347 branch-site test implemented in PAML codeml⁵⁵ independently verified positive selection
348 ($P<0.05$). This revealed 9 genes with a robust signal of positive selection at the bat ancestor
349 (Table S13). While these 9 genes have diverse functions, they included two genes with hearing-
350 related functions, which may relate to the evolution of echolocation. These genes, *LRP2* (low-
351 density lipoprotein receptor-related protein 2, also called megalin) and *SERPINB6* (serpin
352 family B member 6) are expressed in the cochlea and associated with human disorders
353 involving deafness. *LRP2* encodes a multi-ligand receptor involved in endocytosis that is
354 expressed in the kidney, forebrain and, importantly, is also expressed in the cochlear duct⁵⁶.
355 Mutations in this gene are associated with Donnai-Barrow Syndrome, an autosomal recessive
356 disease with symptoms including sensorineural deafness⁵⁷, and progressive hearing loss has
357 also been observed in *Lrp2* knockout mice⁵⁸. Similarly, *SERPINB6* is associated with non-
358 syndromic hearing loss and this serine protease inhibitor is expressed in cochlear hair cells^{59,60}.
359 Sites identified as having experienced positive selection at the bat ancestor showed bat-specific
360 substitutions in both genes. Interestingly, the echolocating bats showed a specific asparagine
361 to methionine substitution in *LRP2*. In *Rousettus*, the only non-laryngeal echolocator in our six
362 bats, this site has been substituted for a threonine. Combined with analysis of 6 other publicly
363 available bat genomes (n=6), we confirmed the presence of a methionine in all laryngeal
364 echolocating bats (n=9) and a threonine residue in all non-echolocating pteropodids (n=3) (Fig.
365 S8).

366
367 We also initially identified positive selection in the bat ancestor in a third hearing-related gene,
368 *TJP2* (tight junction protein 2), that is expressed in cochlear hair cells and associated with
369 hearing loss^{61,62}. However, manual inspection revealed a putative alignment ambiguity and the
370 manually-corrected alignment had a reduced significance (aBSREL raw $P=0.009$, not
371 significant after multiple test correction considering 12,931 genes). Interestingly, the corrected
372 alignment revealed a four amino acid microduplication found only in echolocating bats (n=9)
373 (Fig. S9), which may be explained by incomplete lineage sorting or convergence. It should be
374 noted that insertions and deletions may also affect protein function but are not considered by
375 tests for positive selections, however a phylogenetic interpretation of these events may uncover
376 functional adaptations. In general, experimental studies are required to test whether the pattern
377 of positive selection and bat-specific mutations on the stem Chiroptera branch affect hearing-
378 related functions of these three genes. If so, this would provide molecular support for laryngeal

379 echolocation as a shared ancestral trait of bats and subsequent loss in pteropodids, informing a
380 long-standing debate in bat biology of whether ancestral bats had the ability to echolocate¹².

381
382 In addition to hearing-related genes, our genome-wide screen revealed selection on immunity-
383 related genes, *CXCL13* (C-X-C motif chemokine ligand 13), *NPSR1* (neuropeptide S receptor
384 1) and *INAVA* (innate immunity activator), which may underlie bats' unique tolerance of
385 pathogens⁹. The *CXCL13* (previously B-lymphocyte chemoattractant) protein is a B-cell
386 specific chemokine, which attracts B-cells to secondary lymphoid organs, such as lymph nodes
387 and spleen⁶³. *NPSR1* expresses a receptor activated by neuropeptide S. Activation of *NPSR1*
388 induces an inflammatory immune response in macrophages and *NPSR1* polymorphisms have
389 been associated with asthma in humans⁶⁴. *INAVA* encodes an immunity-related protein with a
390 dual role in innate immunity. In intestinal epithelial cells, this gene is required for intestinal
391 barrier integrity and the repair of epithelial junctions after injury^{65,66}. Consistent with these
392 functions, mutations in human *INAVA* are associated with inflammatory bowel disease⁶⁷, a
393 disorder characterized by chronic inflammation of the gastrointestinal tract and an increased
394 susceptibility to microbial pathogens. In macrophages, *INAVA* amplifies an IL-1 β -induced pro-
395 inflammatory response by enhancing NF- κ B signalling⁶⁶.

396
397 While a genome-wide screen for significant signatures of positive selection is comprehensive,
398 considering 12,931 orthologous genes may reduce sensitivity due to the necessity to correct for
399 12,931 statistical tests. To increase the sensitivity in detecting positive selection in genes
400 relevant for prominent bat traits (i.e. longevity, immunity, metabolism²) we further performed
401 a screen considering 2,453 candidate genes (Table S14) associated with these terms according
402 to Gene Ontology (GO), AmiGO⁶⁸ and GenAge⁶⁹ annotations. This reduced gene set permitted
403 a screen for signatures of positive selection using both the aBSREL model and the branch-site
404 test implemented in codeml (supplementary methods section 4.3.1). Requiring significance by
405 both aBSREL and codeml (FDR<0.05), we found 10 additional genes with robust evidence of
406 positive selection in the ancestral bat lineage (Table S15, Fig. S10). These genes include *IL17D*
407 and *IL-1 β* , which are involved in immune system regulation⁷⁰ and NF- κ B activation (*IL-1 β*)^{66,71}, and *GP2* and *LCN2*, which are involved in the response to pathogens^{72,73}. Interestingly,
409 selection was also inferred for *PURB*, a gene that plays a role in cell proliferation and regulates
410 the oncogene *MYC*⁷⁴, which was previously shown to be under divergent selection in bats¹⁶ and
411 which exhibits a unique anti-ageing transcriptomic profile in long lived *Myotis* bats⁸. Overall,
412 combining genome-wide and candidate gene screens revealed robust patterns of selection in

413 stem Chiroptera on several genes involved in immunity and infection, which suggests that
414 ancestral bats evolved immunomodulatory mechanisms that enabled a higher tolerance to
415 pathogens.

416

417 Second, we used a previously developed approach⁷⁵ to systematically screen for gene loss. This
418 revealed 10 genes that are inactivated in our six bats but present in the majority of
419 Laurasiatheria (Table S16). Two of these genes again point to changes in immune function in
420 bats, having immune-stimulating and pro-inflammatory functions; *LRRC70* (leucine rich repeat
421 containing 70, also called synleurin) and *IL36G* (interleukin 36 gamma) (Fig. 3a). *LRRC70* is
422 expressed in a broad range of tissues and potentiates cellular responses to multiple cytokines⁷⁶
423 and is well conserved among Laurasiatheria. Importantly, *LRRC70* strongly amplifies bacterial
424 lipopolysaccharide-mediated NF- κ B activation⁷⁶. Our finding of *LRRC70* loss in bats makes
425 this poorly characterized gene an interesting target for future mechanistic studies. *IL36G*,
426 encodes a pro-inflammatory interleukin belonging to the interleukin-1 family. Increased
427 expression of *IL36G* was detected in psoriasis and inflammatory bowel disease patients, and
428 *IL36G* is likely involved in the pathophysiology of these diseases by inducing the canonical
429 NF- κ B pathway and other proinflammatory cytokines⁷⁷⁻⁷⁹. Further analysis of common
430 mutations between our assembled genomes and previously published bat genomes (n=9),
431 revealed these genes were in fact lost multiple times within Chiroptera (Fig. S11 and S12),
432 suggesting these genes came under relaxed selection in bats followed by with subsequent gene
433 losses. Together, genome-wide screens for gene loss and positive selection revealed several
434 genes involved in NF- κ B signalling (Fig. 3b), suggesting that altered NF- κ B signalling may
435 contribute to immune related adaptations in bats.

436

437 Third, we investigated changes in gene family size, which revealed 35 cases of significant gene
438 family expansions and contractions at the bat ancestor (Table S17). Among these, we inferred
439 an expansion of the *APOBEC* gene family. Expansion involved *APOBEC3*-type genes (Fig.
440 3c) and supported a small expansion in the ancestral bat lineage, followed by up to 14
441 duplication events within Chiroptera. The *APOBEC3* locus is highly-dynamic, with a complex
442 history of duplication, loss and fusion in Mammalia⁸⁰. Our analysis of this locus in Chiroptera
443 adds to previous evidence of a genus specific expansion in the flying foxes (genus *Pteropus*)⁸¹,
444 showing this locus has undergone many independent expansions in bats. *APOBEC* genes are
445 DNA and RNA editing enzymes with roles in lipoprotein regulation and somatic
446 hypermutation⁸². *APOBEC3*-type genes have been previously associated with restricting viral

447 infection, transposon activity⁸² and may also be stimulated by interferon signalling⁸³.
448 Expansion of *APOBEC3* genes in multiple bat lineages suggests these duplications may
449 contribute to viral tolerance in these lineages.

450
451 **Integrated Viruses in Bat Genomes**

452 There is mounting evidence to suggest that bats are major zoonotic reservoir hosts, as they can
453 tolerate and survive viral infections (e.g. Ebola and MERs), potentially due to adaptations in
454 their immune response⁸⁴, consistent with our findings of selection in immune-related genes
455 (e.g. *INAVA*) and expansions of the viral-restricting *APOBEC3* gene cluster. We screened our
456 high-quality genomes to ascertain the number and diversity of endogenous viral elements
457 (EVEs), considered as ‘molecular fossil’ evidence of ancient infections. Given their retroviral
458 life cycle endogenous retroviruses (ERVs) are the largest group found among all EVEs in
459 vertebrate genomes^{85,86} (making up ~10% of the mouse⁸⁷ and 8% of the human genome⁸⁸),
460 while non-retroviral EVEs are far less numerous in animal genomes⁸⁶.

461
462 Using reciprocal BLAST searches and a custom comprehensive library of viral protein
463 sequences we first screened our six bat genomes and seven mammalian outgroups
464 (supplementary methods section 3.4) for the presence of EVEs, including ERVs and non-
465 retroviral EVEs. We identified three predominant non-retroviral EVE families: *Parvoviridae*,
466 *Adenoviridae* and *Bornaviridae* (Fig. 4a). Parvovirus and bornavirus integrations were found
467 in all bats except for *Rousettus* and *M. molossus* respectively. A partial filovirus EVE was
468 found to be present in the Vespertilionidae (*Pipistrellus* & *Myotis*), but absent in the other bat
469 species, suggesting that vespertilionid bats have been exposed in the past to and can survive
470 filoviral infections, corroborating a previous study⁸⁹.

471
472 Next, we identified retroviral proteins from all ERV classes within the bat genomes. Consistent
473 with other mammals, the highest number of integrations came from beta- and gamma-like
474 retroviruses^{90,91}, with beta-like integrations most common for *pol* and *gag* proteins and gamma-
475 like integrations most common for *env* proteins in most of the bats (Fig. 4b & Fig. S13).
476 Overall, the highest number of integrations was observed in *M. myotis* (n=630), followed by
477 *Rousettus* (n=334) with *Phyllostomus* containing the lowest (n=126; Fig. 4b, Table S18).
478 Additionally, we detected ERV sequences with hits for alpha- and lenti-retroviruses in
479 reciprocal BLAST searches. Until now, alpharetroviruses were considered as exclusively
480 endogenous avian viruses⁹². Thus, our discovery of endogenous alpharetroviral-like elements

481 in bats is the first record of these sequences in mammalian genomes, widening the known
482 biodiversity of potential hosts for retrovirus transmission. We detected several alpha-like *env*
483 regions in *Phyllostomus*, *Rhinolophus*, and *Rousettus* (Fig. 4b), showing that multiple and
484 diverse bat species have been and possibly are being infected by alpharetroviruses. We also
485 detected lentivirus *gag*-like fragments in *Pipistrellus*, which are rarely observed in endogenized
486 form⁹³.

487

488 To identify historical ancestral transmission events, we reconstructed a phylogenetic tree from
489 our recovered ERVs with the known viral protein ‘probe’ sequences for all six bat genomes
490 and seven mammalian outgroups (Fig. S14). The majority of sequences group as single bat-
491 species clusters, suggesting that relatively recent integration events, more than ancestral
492 transmission (Fig. S14) govern the ERV diversity. While, most ERVs are simple retroviruses,
493 consisting of *gag*, *pol* and *env* genes, we found an unusual diversity of complex retroviruses in
494 bats, which are generally rare in endogenous form⁹³⁻⁹⁵ (Fig. S14). We detected a clade of 5
495 *Rhinolophus pol* sequences clustered together with reference foamy retroviruses – Feline
496 Foamy Virus (FFV) and Bovine Foamy Virus (BFV). Foamy retroviruses in bats were detected
497 before from metagenomic data from *Rhinolophus affinis*⁹⁶, however, until now it was unclear
498 whether these sequences represented exogenous or endogenous viruses⁹⁷. With the detection
499 of these sequences, we can now confirm the presence of endogenous spumaretroviruses in the
500 *R. ferrumequinum* genome, which furthers our understanding of the historical transmission
501 dynamics of this pathogen. We also detected *pol* sequences in the *Molossus* genome clustering
502 closely with reference delta sequences (Bovine Leukemia virus – BLV, Human T-
503 lymphotropic Virus – HTLV). *Pol* regions for delta retroviruses in bats have not been detected
504 before, with only partial *gag* and a single LTR identified previously in *Miniopterus* and
505 *Rhinolophus* species^{94,98}.

506

507 Overall these results show that bat genomes contain a surprising diversity of ERVs, with some
508 sequences never previously recorded in mammalian genomes, confirming interactions between
509 bats and complex retroviruses, which endogenize exceptionally rarely. These integrations are
510 indicative of past viral infections, highlighting which viruses bat species have co-evolved with
511 and tolerated, and thus, can help us better predict potential zoonotic spillover events and direct
512 routine viral monitoring in key species and populations. In addition, bats, as one of the largest
513 orders of mammals, are an excellent model to observe how co-evolution with viruses can shape
514 the mammalian genome over evolutionary timescales. For example, the expansion of the

515 *APOBEC3* genes in bats shown herein, could be a result of a co-evolutionary arms race shaped
516 by ancient retroviral invasions, and could contribute to the restriction in copy number of
517 endogenous viruses in some bat species. Given that these findings were generated from only
518 six bat genomes we can be confident that further cross-species comparison with similar quality
519 bat genomes will bring even greater insight.

520
521 **Changes in Non-Coding RNAs**
522 In addition to coding genes, changes in non-coding (nc)RNAs can be associated with
523 interspecific phenotypic variation and can drive adaptation^{99,100}. We used our reference-quality
524 genomes to comprehensively annotate non-coding RNAs and search for ncRNA changes
525 between bat species and other mammals. To annotate different classes of conserved non-coding
526 RNA genes, we used computational methods that capture characteristic sequence and structure
527 features of ncRNAs (Fig. 5a; supplementary methods section 5.1). We found that a large
528 proportion of non-coding RNA genes were shared across all six bats (Fig. S15), and between
529 bats and other mammals (e.g. 95.8% ~ 97.4% shared between bats and human).

530
531 Within ncRNAs, we next investigated microRNAs (miRNA), which can serve as
532 developmental and evolutionary drivers of change¹⁰¹. We employed a strict pipeline to annotate
533 known miRNAs in our six bat genomes and in the 42 outgroup mammal taxa (Table S19,
534 supplementary methods section 5.1) and investigated how the size of miRNA families evolved
535 using CAFÉ¹⁰². We identified 286 miRNA families present in at least one mammal and
536 observed massive contractions of these miRNA families (Fig. S16) with an estimated overall
537 rate of ‘death’ 1.43 times faster than the rate of ‘birth’ (see supplementary methods section
538 5.1). There were 19 families that significantly (FDR<0.05) contracted in the ancestral bat
539 branch, with no evidence of expansions, and between 4 and 35 miRNA families were
540 contracted across bats (Fig. 5b, Fig. S16). We also inferred the miRNA families lost in each
541 bat lineage using a Dollo parsimony approach, which revealed 16 miRNA families that were
542 lost in the bat ancestor (Fig. S17 and S18). Interestingly, the oncogenic miR-374 was lost in all
543 bat species but was found in the other examined orders (Table S19). Since miR-374 promotes
544 tumour progression and metastasis in diverse human cancers¹⁰³, this bat specific loss may
545 contribute to low cancer rates in bats¹⁶.

546
547 Next, we investigated the evolution of single-copy miRNA genes to determine if sequence
548 variation in these miRNAs may be driving biological change. Alignments of 98 highly

549 conserved, single-copy miRNA genes identified across all 48 mammal genomes revealed that
550 one miRNA, miR-337-3p, had unique variation in the seed region in bats compared to all other
551 42 mammals (Fig. 5c). miR-337-3p was pervasively expressed in brain, liver, and kidney across
552 all six bat species (Fig. S19). Given that the seed sequences of microRNAs represent the
553 strongest determinant of target specificity, these changes are expected to alter the repertoire of
554 sequences targeted by miR-337-3p in bats.

555

556 To test this hypothesis, we used reporter assays^{104,105} to determine if the bat and human versions
557 of miR-337-3p were functionally active and if they showed species-specific regulation of an
558 “ideal” predicted target sequence (Table S20). While bat miR-337-3p strongly repressed the
559 expression of its cognate bat target sequence, it had no effect on the human site, and *vice versa*
560 (Fig. 5d). This result demonstrated that the miR-337-3p seed changes found in bats alter its
561 binding specificity. To explore whether this difference in binding specificity changes the set of
562 target genes regulated by bat miR-337-3p, we used our raw Iso-seq data to identify 3'UTRs of
563 coding genes in bats (n=6,891-16,115) and determined possible target genes of miR-337-3p
564 using a custom *in silico* pipeline (Table S21; supplementary methods section 5.3.5). We also
565 obtained the equivalent human 3'UTRs for all predicted bat 3'UTRs and identified the human
566 miR-337-3p gene targets (supplementary methods section 5.3.5). In bats, miR-337-3p was
567 predicted to regulate a distinct spectrum of gene targets compared to humans (Table S22). GO
568 enrichment analysis of these target gene sets suggests a shift towards regulation of
569 developmental, rhythmic, synaptic and behavioural gene pathways by miR-337-3p in bats (Fig.
570 5e), pointing to a dramatic change in processes regulated by miR-337-3p in bats compared to
571 other mammals.

572

573 In addition to losses and changes in miRNAs, continuous miRNA innovation is observed in
574 eukaryotes, which is suggested as a key player in the emergence of increasing organismal
575 complexity⁹⁹. To identify any novel miRNAs that evolved in bats, we performed deep
576 sequencing of small RNA libraries from brain, liver and kidney for all six bats (Table S23),
577 analysed these data using a comprehensive custom analysis pipeline (see supplementary
578 methods section 5.3.3), and identified those miRNAs that possess seed regions not found in
579 miRBase (release 22). This screen revealed between 122 and 261 novel miRNAs across the six
580 bat genomes. Only a small number of these novel miRNAs were shared across the six bats,
581 supporting rapid birth of miRNAs on bat lineages (Fig. S20). We identified 12 novel miRNAs
582 that were found in all six bats but did not have apparent homologs in other mammals (Table

583 S24). Prediction of miRNAs from genomic sequences alone may result in false positives due
584 to the occurrence of short hairpin-forming sequences that are predicted to form hairpins but are
585 not processed or functionally active, emphasizing the need for experimental testing of these
586 miRNAs. Therefore, to test whether these candidates indeed function as miRNAs we selected
587 the top 3 candidates (bat-miR-4665, bat-miR-19125, bat-miR-6665) (Table S24) based on their
588 expression and secondary structures, and experimentally tested their ability to regulate an ideal
589 target sequence in reporter assays, as above (Table S20). Two of the three miRNAs (miR-
590 19125 and miR-6665) were able to regulate their targets, showing that they are actively
591 processed by the endogenous miRNA machinery, and able to be loaded onto the RISC complex
592 to repress target mRNAs (Fig. 5f). Thus, miR-19125 and miR-6665 represent true miRNAs
593 that are novel to bats. Taken together, these data demonstrate innovation in the bat lineage with
594 regard to miRNAs both in seed sequence variation as well as novel miRNA emergence.

595

596 In summary, our genomic screens and experiments revealed losses of ancestral miRNAs, gains
597 of novel functional miRNA and a striking case of miRNA seed change that alters the target
598 specificity. Changes in these miRNAs and their target genes point to a regulatory role in cancer,
599 development and behaviour in bats. Further detailed mechanistic studies will be crucial to
600 determine the role of these miRNAs in bat physiology and evolution.

601

602 **Discussion**

603 We have used a combination of state-of-the-art methods including long-read, short-read, and
604 scaffolding technologies to generate chromosome level, near-complete assemblies of six bats
605 that represent diversity within Chiroptera. These reference-quality genomes improve on all
606 published bat genomes and are on par with the best reference-quality genomes currently
607 generated for any eukaryotic species with a complex, multi-gigabyte genome. Compared to the
608 contiguity and completeness of previous bat genomes assembled with short reads, our
609 reference-quality genomes offer significant advances. First, while fragmented and incomplete
610 assemblies hamper gene annotation, reference-quality genomes allow comprehensive
611 annotations by integrating a variety of methods and evidence. In particular, reference-quality
612 genomes facilitate genome alignment, which provides a powerful way of transferring gene
613 annotations of related species to new assemblies and ensures that transcriptomic data can be
614 comprehensively mapped. Second, while fragmented and incomplete assemblies resulted in
615 countless efforts by individual labs to laboriously clone and re-sequence genomic loci
616 containing genes of interest, such efforts are not necessary with comprehensively annotated,

617 reference-quality assemblies. Third, reference-quality assemblies are a resource for studying
618 gene regulation by non-coding RNAs and cis-regulatory elements. The high completeness
619 enables a comprehensive mapping of functional genomics data such as miRNA read data and
620 epigenomic data (e.g. ChIP-seq, ATAC-Seq), and the high contiguity is crucial for assigning
621 regulatory regions to putative target genes and linking genotype to phenotype.

622

623 The six reference-quality assemblies coupled with methodological advances enabled us to
624 address the long-standing question of the phylogenetic position of bats within Laurasiatheria.
625 We used our comprehensive gene annotations to obtain the largest set of orthologous genes
626 and homologous regions to date, which enabled us to explore the phylogenetic signal across
627 different genomic partitions. Consistently, a variety of phylogenetic methods and data sets
628 estimate that bats are a sister clade to Fereungulata and highlight the importance of
629 maximising the genetic coverage and ensuring that the appropriate models and data are used
630 when reconstructing difficult nodes.

631

632 Our comprehensive and conservative genome-wide screens investigating gene gain, loss and
633 selection provide candidates that are likely related to the unique immunity of bats. Furthermore,
634 our screens reveal selection in hearing genes in stem Chiroptera, which is consistent with the
635 hypothesis that echolocation evolved once in bats and was secondarily lost in Pteropodidae,
636 but inconsistent with the alternative hypothesis that echolocation evolved twice independently
637 within bats. As such, our analysis provides molecular evidence informing a long-standing
638 question of when echolocation evolved. We further show that bats have a long coevolutionary
639 history with viruses and identified unique mammalian viral integrations. Finally, we explored
640 the non-coding genome in bats, where we found miRNAs that were novel to bats, lost in bats,
641 or carried bat specific changes in their seed sequence. These important regulators of gene
642 expression point to ancestral changes in the bat genome that may have contributed to
643 adaptations related to the low incidence of cancer in bats, as well as developmental and
644 behavioural processes.

645

646 While the six bat genomes presented here are an excellent starting point to understand the
647 evolution of exceptional traits in bats, questions remain to be addressed in future studies,
648 particularly because bats as a group exhibit such an incredible diversity. To resolve the
649 phylogeny of the 21 currently-recognized bat families and to further understand the evolution
650 and molecular mechanisms of traits that vary among bat families, such as longevity, mode of

651 echolocation or diet, the Bat1K project aims at producing, in its next phase, reference-quality
652 assemblies for at least one member of each of the 21 bat families. To enable efficient use of
653 our reference-quality genomes, we provide all genomic and transcriptomic data together with
654 all annotation and genome alignment in an open access genome browser (<https://genome-public.pks.mpg.de>) for download and visualization. These, and future bat genomes are
655 expected to provide a rich resource by which to address the evolution of the extraordinary
656 adaptations in bats and contribute to our understanding of key phenotypes including those
657 relevant for human health and disease.

659 **References**

660 1 Lazzeroni, M. E., Burbrink, F. T. & Simmons, N. B. Hibernation in bats (Mammalia:
661 Chiroptera) did not evolve through positive selection of leptin. *Ecol Evol* **8**, 12576-
662 12596, doi:10.1002/ece3.4674 (2018).

663 2 Teeling, E. C. *et al.* Bat Biology, Genomes, and the Bat1K Project: To Generate
664 Chromosome-Level Genomes for All Living Bat Species. *Annu Rev Anim Biosci* **6**, 23-
665 46, doi:10.1146/annurev-animal-022516-022811 (2018).

666 3 Kacprzyk, J. *et al.* A potent anti-inflammatory response in bat macrophages may be
667 linked to extended longevity and viral tolerance. *Acta chiropterologica* **19**, 219-228
668 (2017).

669 4 Ahn, M., Cui, J., Irving, A. T. & Wang, L. F. Unique Loss of the PYHIN Gene Family
670 in Bats Amongst Mammals: Implications for Inflammasome Sensing. *Sci Rep* **6**, 21722,
671 doi:10.1038/srep21722 (2016).

672 5 O'Shea, T. J. *et al.* Bat flight and zoonotic viruses. *Emerg Infect Dis* **20**, 741-745,
673 doi:10.3201/eid2005.130539 (2014).

674 6 Brook, C. E. & Dobson, A. P. Bats as 'special' reservoirs for emerging zoonotic
675 pathogens. *Trends Microbiol* **23**, 172-180, doi:10.1016/j.tim.2014.12.004 (2015).

676 7 Wilkinson, G. S. & Adams, D. M. Recurrent evolution of extreme longevity in bats.
677 *Biol Lett* **15**, 20180860, doi:10.1098/rsbl.2018.0860 (2019).

678 8 Huang, Z. *et al.* Longitudinal comparative transcriptomics reveals unique mechanisms
679 underlying extended healthspan in bats. *Nat Ecol Evol* **3**, 1110-1120,
680 doi:10.1038/s41559-019-0913-3 (2019).

681 9 Mandl, J. N., Schneider, C., Schneider, D. S. & Baker, M. L. Going to Bat(s) for Studies
682 of Disease Tolerance. *Front Immunol* **9**, 2112, doi:10.3389/fimmu.2018.02112 (2018).

683 10 Jones, G., Teeling, E. C. & Rossiter, S. J. From the ultrasonic to the infrared: molecular
684 evolution and the sensory biology of bats. *Front Physiol* **4**, 117,
685 doi:10.3389/fphys.2013.00117 (2013).

686 11 Vernes, S. C. What bats have to say about speech and language. *Psychon Bull Rev* **24**,
687 111-117, doi:10.3758/s13423-016-1060-3 (2017).

688 12 Wang, Z. *et al.* Prenatal development supports a single origin of laryngeal echolocation
689 in bats. *Nat Ecol Evol* **1**, 21, doi:10.1038/s41559-016-0021 (2017).

690 13 Brown, E. E., Cashmore, D. D., Simmons, N. B. & Butler, R. J. Quantifying the
691 completeness of the bat fossil record. *Palaeontology* (2019).

692 14 Foley, N. M., Springer, M. S. & Teeling, E. C. Mammal madness: is the mammal tree
693 of life not yet resolved? *Philos Trans R Soc Lond B Biol Sci* **371**,
694 doi:10.1098/rstb.2015.0140 (2016).

695 15 Teeling, E. C. *et al.* A molecular phylogeny for bats illuminates biogeography and the
696 fossil record. *Science* **307**, 580-584, doi:10.1126/science.1105113 (2005).

697 16 Foley, N. M. *et al.* Growing old, yet staying young: The role of telomeres in bats'
698 exceptional longevity. *Sci Adv* **4**, eaao0926, doi:10.1126/sciadv.aa0926 (2018).

699 17 Hayman, D. T. Bats as Viral Reservoirs. *Annu Rev Virol* **3**, 77-99, doi:10.1146/annurev-
700 virology-110615-042203 (2016).

701 18 Nowoshilow, S. *et al.* The axolotl genome and the evolution of key tissue formation
702 regulators. *Nature* **554**, 50-55, doi:10.1038/nature25458 (2018).

703 19 Tischler, G. Haplotype and Repeat Separation in Long Reads. *bioRxiv*, 145474,
704 doi:10.1101/145474 (2017).

705 20 Tischler, G. & Myers, E. W. Non hybrid long read consensus using local de Bruijn
706 graph assembly. *bioRxiv*, 106252 (2017).

707 21 Eckalbar, W. L. *et al.* Transcriptomic and epigenomic characterization of the
708 developing bat wing. *Nat Genet* **48**, 528-536, doi:10.1038/ng.3537 (2016).

709 22 Pavlovich, S. S. *et al.* The Egyptian Rousette Genome Reveals Unexpected Features of
710 Bat Antiviral Immunity. *Cell* **173**, 1098-1110 e1018, doi:10.1016/j.cell.2018.03.070
711 (2018).

712 23 Koren, S. *et al.* De novo assembly of haplotype-resolved genomes with trio binning.
713 *Nat Biotechnol*, doi:10.1038/nbt.4277 (2018).

714 24 Nature Biotechnology Editorial. A reference standard for genome biology. *Nat
715 Biotechnol* **36**, 1121, doi:10.1038/nbt.4318 (2018).

716 25 Waterhouse, R. M. *et al.* BUSCO applications from quality assessments to gene
717 prediction and phylogenomics. *Mol Biol Evol*, doi:10.1093/molbev/msx319 (2017).

718 26 Bejerano, G. *et al.* Ultraconserved elements in the human genome. *Science* **304**, 1321-
719 1325, doi:10.1126/science.1098119 (2004).

720 27 Aken, B. L. *et al.* The Ensembl gene annotation system. *Database (Oxford)* **2016**,
721 doi:10.1093/database/baw093 (2016).

722 28 Sharma, V., Schwede, P. & Hiller, M. CESAR 2.0 substantially improves speed and
723 accuracy of comparative gene annotation. *Bioinformatics* **33**, 3985-3987,
724 doi:10.1093/bioinformatics/btx527 (2017).

725 29 Stanke, M., Schoffmann, O., Morgenstern, B. & Waack, S. Gene prediction in
726 eukaryotes with a generalized hidden Markov model that uses hints from external
727 sources. *BMC Bioinformatics* **7**, 62, doi:10.1186/1471-2105-7-62 (2006).

728 30 Kuo, R. I., Cheng, Y., Smith, J., Archibald, A. L. & Burt, D. W. Illuminating the dark
729 side of the human transcriptome with TAMA Iso-Seq analysis. *bioRxiv* (2019).

730 31 Platt, R. N., 2nd, Blanco-Berdugo, L. & Ray, D. A. Accurate Transposable Element
731 Annotation Is Vital When Analyzing New Genome Assemblies. *Genome Biol Evol* **8**,
732 403-410, doi:10.1093/gbe/evw009 (2016).

733 32 Pace, J. K., 2nd & Feschotte, C. The evolutionary history of human DNA transposons:
734 evidence for intense activity in the primate lineage. *Genome Res* **17**, 422-432,
735 doi:10.1101/gr.5826307 (2007).

736 33 Platt, R. N., 2nd, Mangum, S. F. & Ray, D. A. Pinpointing the vesper bat transposon
737 revolution using the *Miniopterus natalensis* genome. *Mob DNA* **7**, 12,
738 doi:10.1186/s13100-016-0071-y (2016).

739 34 Doronina, L. *et al.* Speciation network in Laurasiatheria: retrophylogenomic signals.
740 *Genome Res* **27**, 997-1003, doi:10.1101/gr.210948.116 (2017).

741 35 Springer, M. S. & Gatesy, J. An ABBA-BABA Test for Introgression Using
742 Retroposon Insertion Data. *bioRxiv*, doi:10.1101/709477 (2019).

743 36 Kalyaanamoorthy, S., Minh, B. Q., Wong, T. K. F., von Haeseler, A. & Jermiin, L. S.
744 ModelFinder: fast model selection for accurate phylogenetic estimates. *Nat Methods*
745 **14**, 587-589, doi:10.1038/nmeth.4285 (2017).

746 37 Nguyen, L. T., Schmidt, H. A., von Haeseler, A. & Minh, B. Q. IQ-TREE: a fast and
747 effective stochastic algorithm for estimating maximum-likelihood phylogenies. *Mol
748 Biol Evol* **32**, 268-274, doi:10.1093/molbev/msu300 (2015).

749 38 Tarver, J. E. *et al.* The Interrelationships of Placental Mammals and the Limits of
750 Phylogenetic Inference. *Genome Biol Evol* **8**, 330-344, doi:10.1093/gbe/evv261 (2016).

751 39 Hoang, D. T., Chernomor, O., von Haeseler, A., Minh, B. Q. & Vinh, L. S. UFBoot2:
752 Improving the Ultrafast Bootstrap Approximation. *Mol Biol Evol* **35**, 518-522,
753 doi:10.1093/molbev/msx281 (2018).

754 40 Nishihara, H., Hasegawa, M. & Okada, N. Pegasoferae, an unexpected mammalian
755 clade revealed by tracking ancient retroposon insertions. *Proc Natl Acad Sci U S A* **103**,
756 9929-9934, doi:10.1073/pnas.0603797103 (2006).

757 41 Tsagkogeorga, G., Parker, J., Stupka, E., Cotton, J. A. & Rossiter, S. J. Phylogenomic
758 analyses elucidate the evolutionary relationships of bats. *Curr Biol* **23**, 2262-2267,
759 doi:10.1016/j.cub.2013.09.014 (2013).

760 42 Jermiin, L. S., Poladian, L. & Charleston, M. A. Evolution. Is the "Big Bang" in animal
761 evolution real? *Science* **310**, 1910-1911, doi:10.1126/science.1122440 (2005).

762 43 Philippe, H. *et al.* Resolving difficult phylogenetic questions: why more sequences are
763 not enough. *PLoS Biol* **9**, e1000602, doi:10.1371/journal.pbio.1000602 (2011).

764 44 Zhang, G. *et al.* Comparative genomics reveals insights into avian genome evolution
765 and adaptation. *Science* **346**, 1311-1320, doi:10.1126/science.1251385 (2014).

766 45 Degnan, J. H. & Rosenberg, N. A. Discordance of species trees with their most likely
767 gene trees. *PLoS Genet* **2**, e68, doi:10.1371/journal.pgen.0020068 (2006).

768 46 Charlesworth, B. Fundamental concepts in genetics: effective population size and
769 patterns of molecular evolution and variation. *Nat Rev Genet* **10**, 195-205,
770 doi:10.1038/nrg2526 (2009).

771 47 Hobolth, A., Andersen, L. N. & Mailund, T. On computing the coalescence time density
772 in an isolation-with-migration model with few samples. *Genetics* **187**, 1241-1243,
773 doi:10.1534/genetics.110.124164 (2011).

774 48 Jermiin, L. S., Jayaswal, V., Ababneh, F. M. & Robinson, J. Identifying Optimal
775 Models of Evolution. *Methods Mol Biol* **1525**, 379-420, doi:10.1007/978-1-4939-6622-
776 6_15 (2017).

777 49 Dornburg, A., Su, Z. & Townsend, J. P. Optimal Rates for Phylogenetic Inference and
778 Experimental Design in the Era of Genome-Scale Data Sets. *Syst Biol* **68**, 145-156,
779 doi:10.1093/sysbio/syy047 (2019).

780 50 Ababneh, F., Jermiin, L. S., Ma, C. & Robinson, J. Matched-pairs tests of homogeneity
781 with applications to homologous nucleotide sequences. *Bioinformatics* **22**, 1225-1231,
782 doi:10.1093/bioinformatics/btl064 (2006).

783 51 Chifman, J. & Kubatko, L. Quartet inference from SNP data under the coalescent
784 model. *Bioinformatics* **30**, 3317-3324, doi:10.1093/bioinformatics/btu530 (2014).

785 52 Chou, J. *et al.* A comparative study of SVDquartets and other coalescent-based species
786 tree estimation methods. *BMC Genomics* **16 Suppl 10**, S2, doi:10.1186/1471-2164-16-
787 S10-S2 (2015).

788 53 Smith, M. D. *et al.* Less is more: an adaptive branch-site random effects model for
789 efficient detection of episodic diversifying selection. *Mol Biol Evol* **32**, 1342-1353,
790 doi:10.1093/molbev/msv022 (2015).

791 54 Pond, S. L., Frost, S. D. & Muse, S. V. HyPhy: hypothesis testing using phylogenies.
792 *Bioinformatics* **21**, 676-679, doi:10.1093/bioinformatics/bti079 (2005).

793 55 Yang, Z. PAML 4: phylogenetic analysis by maximum likelihood. *Molecular biology
794 and evolution* **24**, 1586-1591 (2007).

795 56 Mizuta, K. *et al.* Ultrastructural localization of megalin in the rat cochlear duct. *Hear
796 Res* **129**, 83-91, doi:10.1016/s0378-5955(98)00221-4 (1999).

797 57 Kantarci, S. *et al.* Mutations in LRP2, which encodes the multiligand receptor megalin,
798 cause Donnai-Barrow and facio-oculo-acoustico-renal syndromes. *Nat Genet* **39**, 957-
799 959, doi:10.1038/ng2063 (2007).

800 58 Konig, O. *et al.* Estrogen and the inner ear: megalin knockout mice suffer progressive
801 hearing loss. *FASEB J* **22**, 410-417, doi:10.1096/fj.07-9171com (2008).

802 59 Sirmaci, A. *et al.* A truncating mutation in SERPINB6 is associated with autosomal-
803 recessive nonsyndromic sensorineural hearing loss. *Am J Hum Genet* **86**, 797-804,
804 doi:10.1016/j.ajhg.2010.04.004 (2010).

805 60 Tan, J., Prakash, M. D., Kaiserman, D. & Bird, P. I. Absence of SERPINB6A causes
806 sensorineural hearing loss with multiple histopathologies in the mouse inner ear. *Am J*
807 *Pathol* **183**, 49-59, doi:10.1016/j.ajpath.2013.03.009 (2013).

808 61 Walsh, T. *et al.* Genomic duplication and overexpression of TJP2/ZO-2 leads to altered
809 expression of apoptosis genes in progressive nonsyndromic hearing loss DFNA51. *Am*
810 *J Hum Genet* **87**, 101-109, doi:10.1016/j.ajhg.2010.05.011 (2010).

811 62 Hilgert, N. *et al.* Mutation analysis of TMC1 identifies four new mutations and suggests
812 an additional deafness gene at loci DFNA36 and DFNB7/11. *Clin Genet* **74**, 223-232,
813 doi:10.1111/j.1399-0004.2008.01053.x (2008).

814 63 Gunn, M. D. *et al.* A B-cell-homing chemokine made in lymphoid follicles activates
815 Burkitt's lymphoma receptor-1. *Nature* **391**, 799-803, doi:10.1038/35876 (1998).

816 64 Vendelin, J. *et al.* Downstream target genes of the neuropeptide S-NPSR1 pathway.
817 *Hum Mol Genet* **15**, 2923-2935, doi:10.1093/hmg/ddl234 (2006).

818 65 Mohanan, V. *et al.* C1orf106 is a colitis risk gene that regulates stability of epithelial
819 adherens junctions. *Science* **359**, 1161-1166, doi:10.1126/science.aan0814 (2018).

820 66 Luong, P. *et al.* INAVA-ARNO complexes bridge mucosal barrier function with
821 inflammatory signaling. *eLife* **7**, doi:10.7554/eLife.38539 (2018).

822 67 Jostins, L. *et al.* Host-microbe interactions have shaped the genetic architecture of
823 inflammatory bowel disease. *Nature* **491**, 119-124, doi:10.1038/nature11582 (2012).

824 68 Carbon, S. *et al.* AmiGO: online access to ontology and annotation data. *Bioinformatics*
825 **25**, 288-289 (2008).

826 69 de Magalhaes, J. P. & Toussaint, O. GenAge: a genomic and proteomic network map
827 of human ageing. *FEBS letters* **571**, 243-247 (2004).

828 70 Saddawi-Konefka, R. *et al.* Nrf2 Induces IL-17D to Mediate Tumor and Virus
829 Surveillance. *Cell Rep* **16**, 2348-2358, doi:10.1016/j.celrep.2016.07.075 (2016).

830 71 Barker, B. R., Taxman, D. J. & Ting, J. P. Cross-regulation between the IL-1beta/IL-
831 18 processing inflammasome and other inflammatory cytokines. *Curr Opin Immunol*
832 **23**, 591-597, doi:10.1016/j.co.2011.07.005 (2011).

833 72 Flo, T. H. *et al.* Lipocalin 2 mediates an innate immune response to bacterial infection
834 by sequestrating iron. *Nature* **432**, 917-921, doi:10.1038/nature03104 (2004).

835 73 Hase, K. *et al.* Uptake through glycoprotein 2 of FimH(+) bacteria by M cells initiates
836 mucosal immune response. *Nature* **462**, 226-230, doi:10.1038/nature08529 (2009).

837 74 Xu-Monette, Z. Y. *et al.* Clinical and Biologic Significance of MYC Genetic Mutations
838 in De Novo Diffuse Large B-cell Lymphoma. *Clin Cancer Res* **22**, 3593-3605,
839 doi:10.1158/1078-0432.CCR-15-2296 (2016).

840 75 Sharma, V. *et al.* A genomics approach reveals insights into the importance of gene
841 losses for mammalian adaptations. *Nat Commun* **9**, 1215, doi:10.1038/s41467-018-
842 03667-1 (2018).

843 76 Wang, W., Yang, Y., Li, L. & Shi, Y. Synleurin, a novel leucine-rich repeat protein that
844 increases the intensity of pleiotropic cytokine responses. *Biochem Biophys Res*
845 *Commun* **305**, 981-988, doi:10.1016/s0006-291x(03)00876-3 (2003).

846 77 Johnston, A. *et al.* IL-1F5, -F6, -F8, and -F9: a novel IL-1 family signaling system that
847 is active in psoriasis and promotes keratinocyte antimicrobial peptide expression. *J*
848 *Immunol* **186**, 2613-2622, doi:10.4049/jimmunol.1003162 (2011).

849 78 Nishida, A. *et al.* Increased Expression of Interleukin-36, a Member of the Interleukin-
850 1 Cytokine Family, in Inflammatory Bowel Disease. *Inflamm Bowel Dis* **22**, 303-314,
851 doi:10.1097/MIB.0000000000000654 (2016).

852 79 Bridgewood, C. *et al.* IL-36gamma has proinflammatory effects on human endothelial
853 cells. *Exp Dermatol* **26**, 402-408, doi:10.1111/exd.13228 (2017).

854 80 Munk, C., Willemse, A. & Bravo, I. G. An ancient history of gene duplications,
855 fusions and losses in the evolution of APOBEC3 mutators in mammals. *BMC Evol Biol*
856 **12**, 71, doi:10.1186/1471-2148-12-71 (2012).

857 81 Hayward, J. A. *et al.* Differential Evolution of Antiretroviral Restriction Factors in
858 Pteropid Bats as Revealed by APOBEC3 Gene Complexity. *Mol Biol Evol* **35**, 1626-
859 1637, doi:10.1093/molbev/msy048 (2018).

860 82 Salter, J. D., Bennett, R. P. & Smith, H. C. The APOBEC Protein Family: United by
861 Structure, Divergent in Function. *Trends Biochem Sci* **41**, 578-594,
862 doi:10.1016/j.tibs.2016.05.001 (2016).

863 83 Roper, N. *et al.* APOBEC Mutagenesis and Copy-Number Alterations Are Drivers of
864 Proteogenomic Tumor Evolution and Heterogeneity in Metastatic Thoracic Tumors.
865 *Cell Rep* **26**, 2651-2666 e2656, doi:10.1016/j.celrep.2019.02.028 (2019).

866 84 Subudhi, S., Rapin, N. & Misra, V. Immune System Modulation and Viral Persistence
867 in Bats: Understanding Viral Spillover. *Viruses* **11**, doi:10.3390/v11020192 (2019).

868 85 Aswad, A. & Katzourakis, A. Paleovirology and virally derived immunity. *Trends Ecol
869 Evol* **27**, 627-636, doi:10.1016/j.tree.2012.07.007 (2012).

870 86 Katzourakis, A. & Gifford, R. J. Endogenous viral elements in animal genomes. *PLoS
871 Genet* **6**, e1001191, doi:10.1371/journal.pgen.1001191 (2010).

872 87 Mouse Genome Sequencing, C. *et al.* Initial sequencing and comparative analysis of
873 the mouse genome. *Nature* **420**, 520-562, doi:10.1038/nature01262 (2002).

874 88 Lander, E. S. *et al.* Initial sequencing and analysis of the human genome. *Nature* **409**,
875 860-921, doi:10.1038/35057062 (2001).

876 89 Taylor, D. J., Dittmar, K., Ballinger, M. J. & Bruenn, J. A. Evolutionary maintenance
877 of filovirus-like genes in bat genomes. *BMC Evol Biol* **11**, 336, doi:10.1186/1471-2148-
878 11-336 (2011).

879 90 Hayward, A., Grabherr, M. & Jern, P. Broad-scale phylogenomics provides insights
880 into retrovirus-host evolution. *Proc Natl Acad Sci U S A* **110**, 20146-20151,
881 doi:10.1073/pnas.1315419110 (2013).

882 91 Skirmuntt, E. C. & Katzourakis, A. The evolution of endogenous retroviral envelope
883 genes in bats and their potential contribution to host biology. *Virus Res* **270**, 197645,
884 doi:10.1016/j.virusres.2019.197645 (2019).

885 92 Xu, X., Zhao, H., Gong, Z. & Han, G. Z. Endogenous retroviruses of non-
886 avian/mammalian vertebrates illuminate diversity and deep history of retroviruses.
887 *PLoS Pathog* **14**, e1007072, doi:10.1371/journal.ppat.1007072 (2018).

888 93 Katzourakis, A., Tristem, M., Pybus, O. G. & Gifford, R. J. Discovery and analysis of
889 the first endogenous lentivirus. *Proc Natl Acad Sci U S A* **104**, 6261-6265,
890 doi:10.1073/pnas.0700471104 (2007).

891 94 Farkasova, H. *et al.* Discovery of an endogenous Deltaretrovirus in the genome of long-
892 fingered bats (Chiroptera: Miniopteridae). *Proc Natl Acad Sci U S A* **114**, 3145-3150,
893 doi:10.1073/pnas.1621224114 (2017).

894 95 Katzourakis, A., Gifford, R. J., Tristem, M., Gilbert, M. T. & Pybus, O. G.
895 Macroevolution of complex retroviruses. *Science* **325**, 1512,
896 doi:10.1126/science.1174149 (2009).

897 96 Wu, Z. *et al.* Virome analysis for identification of novel mammalian viruses in bat
898 species from Chinese provinces. *J Virol* **86**, 10999-11012, doi:10.1128/JVI.01394-12
899 (2012).

900 97 Katzourakis, A. *et al.* Larger mammalian body size leads to lower retroviral activity.
901 *PLoS Pathog* **10**, e1004214, doi:10.1371/journal.ppat.1004214 (2014).

902 98 Hron, T. *et al.* Remnants of an Ancient Deltaretrovirus in the Genomes of Horseshoe
903 Bats (Rhinolophidae). *Viruses* **10**, doi:10.3390/v10040185 (2018).

904 99 Berezikov, E. Evolution of microRNA diversity and regulation in animals. *Nat Rev Genet* **12**, 846-860, doi:10.1038/nrg3079 (2011).

905 100 Heimberg, A. M., Sempere, L. F., Moy, V. N., Donoghue, P. C. & Peterson, K. J. MicroRNAs and the advent of vertebrate morphological complexity. *Proc Natl Acad Sci U S A* **105**, 2946-2950, doi:10.1073/pnas.0712259105 (2008).

906 101 Moran, Y., Agron, M., Praher, D. & Technau, U. The evolutionary origin of plant and animal microRNAs. *Nat Ecol Evol* **1**, 27, doi:10.1038/s41559-016-0027 (2017).

907 102 De Bie, T., Cristianini, N., Demuth, J. P. & Hahn, M. W. CAFE: a computational tool for the study of gene family evolution. *Bioinformatics* **22**, 1269-1271, doi:10.1093/bioinformatics/btl097 (2006).

908 103 Zhang, J. *et al.* Upregulation of miR-374a promotes tumor metastasis and progression by downregulating LACTB and predicts unfavorable prognosis in breast cancer. *Cancer Med*, doi:10.1002/cam4.1576 (2018).

909 104 Devanna, P., van de Vorst, M., Pfundt, R., Gilissen, C. & Vernes, S. C. Genome-wide investigation of an ID cohort reveals de novo 3'UTR variants affecting gene expression. *Hum Genet* **137**, 717-721, doi:10.1007/s00439-018-1925-9 (2018).

910 105 Devanna, P. *et al.* Next-gen sequencing identifies non-coding variation disrupting miRNA-binding sites in neurological disorders. *Mol Psychiatry* **23**, 1375-1384, doi:10.1038/mp.2017.30 (2018).

911 923

924 **Data availability statement**

925 All data generated or analysed during this study are included in this published article and its
926 supplementary information files. All genomic and transcriptomic data are publicly available
927 for visualization and download via the open-access Bat1K genome browser (<https://genome-public.pks.mpg.de>). In addition, the assemblies have been deposited in the NCBI database and
928 GenomeArk (<https://vgp.github.io/genomeark/>). Accession numbers for all data deposits can
929 be found in the supplementary information files of this article.

930 931

932 **Code availability statement**

933 All code has been made available on github. Details of the location can be found in the
934 supplementary information files of this article. Other custom software is available upon
935 request.

936

937 **Author contributions**

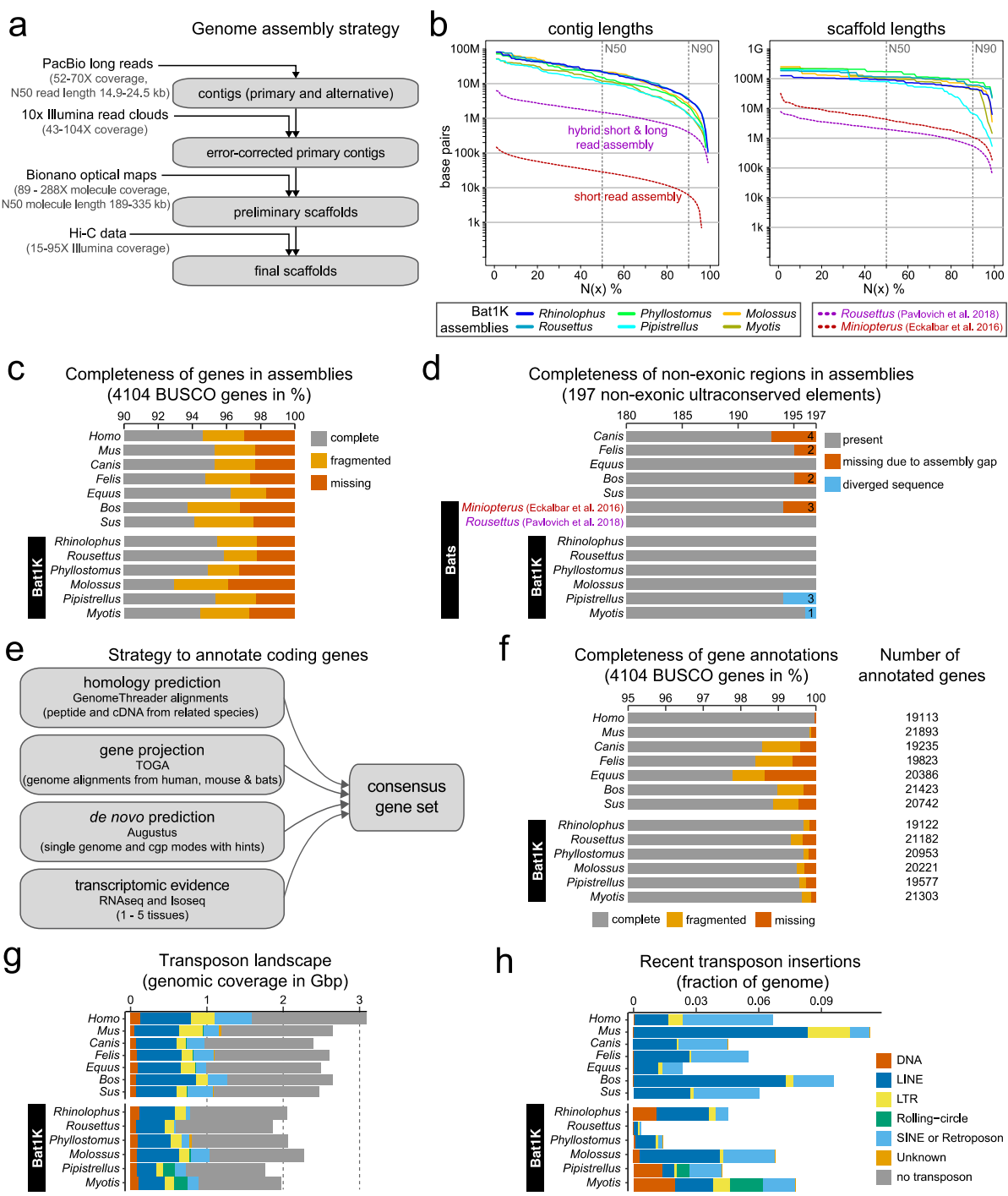
938 MH, SCV, EWM and ECT conceived and supervised the project. MH, SCV, EWM and ECT
939 provided funding. MLP, SJP, DD, GJ, RDR, AGL, ECT and SCV provided tissue samples for
940 sequencing. ZH, JGR, OF and SW were responsible for nucleic acid extraction and sequencing.
941 MP assembled and curated all genomes. DJ provided coding gene annotation and was
942 responsible for coding gene evolutionary analysis. DJ provided multiple sequence and genome
943 alignments. MH and DJ analysed UCE and genome completeness. DJ and MH established the

944 Bat1K genome browser. ZH provided non-coding gene annotation and was responsible for
945 non-coding gene evolutionary analysis. KL processed Iso-seq data and provided UTR
946 annotation. ZH, KL, PD and SCV conducted miRNA target prediction and gene ontology
947 enrichment. PD conducted miRNA functional experiments. GMH, LSJ, MS and ECT provided
948 phylogenomic analyses. GMH and LMD were responsible for codeml analysis. DJ, MH, ZH,
949 GMH, ECT, LMD and AP interpreted evolutionary analyses. BMK and MH developed the
950 TOGA gene projection tool and BMK provided projections for non-bat mammals. ECS, LBG
951 and AK provided EVE annotation and analysis. DR and KAMS provided TE annotation and
952 analysis. EDJ provided support for sequencing of *Phyllostomus* and *Rhinolophus* genomes. DJ,
953 ZH, MP, GH, MH, SCV, EWM and ECT wrote the manuscript. All authors provided edit and
954 comment.

955

956 **Acknowledgements**

957 This work was supported by the Max Planck Society, the German Research Foundation (HI
958 1423/3-1), and by European Research Council Research Grant (ERC-2012-StG311000). SCV
959 was funded by a Max Planck Research Group Award, and a Human Frontiers Science Program
960 (HFSP) Research grant (RGP0058/2016). GJ/ECT – funding from Royal Society/Royal Irish
961 Academy cost share programme. LMD was supported, in part, by NSF-DEB 1442142 and
962 1838273, and NSF-DGE 1633299. DAR was supported, in part, by NSF-DEB 1838283. The
963 authors would like to thank Stony Brook Research Computing and Cyberinfrastructure, and
964 the Institute for Advanced Computational Science at Stony Brook University for access to the
965 high-performance SeaWulf computing system, which was made possible by a National Science
966 Foundation grant (#1531492). ECT was funded by a European Research Council Research
967 Grant (ERC-2012-StG311000), UCD Wellcome Institutional Strategic Support Fund, financed
968 jointly by University College Dublin and SFI-HRB-Wellcome Biomedical Research
969 Partnership (ref 204844/Z/16/Z) and Irish Research Council Consolidator Laureate Award.
970 EDJ and OF were funded by the Rockefeller University and the Howard Hughes Medical
971 Institute. We thank the Long Read Team of the DRESDEN-concept Genome Center, DFG
972 NGS Competence Center, c/o Center for Molecular and Cellular Bioengineering (CMCB),
973 Technische Universität Dresden, Dresden, Germany, Sven Kuenzel and his team of the Max-
974 Planck Institute of Evolutionary Biology in Ploen, Germany, the members of the Vertebrate
975 Genomes Laboratory at The Rockefeller University, New York, US for their support. Special
976 thanks to Lutz Wiegreb, Uwe Firzlaff and Michael Yartsev who gave us access to captive
977 colonies of *Phyllostomus* and *Rousettus* bats and aided with tissue sample collection.



978
979
980 **Figure 1: Assembly and annotation of the genomes of six bats.** (a) Genome assembly
981 strategy and the amount of data produced for assembling contigs and scaffolds. (b) Comparison
982 of assembly contiguity. N(x)% graphs show the contig (left) and scaffold (right) sizes (y-axis),
983 where x% of the assembly consists of contigs and scaffolds of at least that size. Dashed lines
984 show contiguities of two recent bat assemblies, *Miniopterus* generated from short read data²¹,
985 and *Roussettus* generated from a hybrid of short and long read data²². (c) Comparison of
986 coding gene completeness. Bar charts show the percent of 4104 highly-conserved mammalian BUSCO
987 genes that are completely present, fragmented or missing in the assembly. (d) Comparison of
988 completeness in non-exonic regions. Bar charts show the number of detected ultraconserved
989 elements that align at stringent parameters. Ultraconserved elements not detected are separated
990 into those that are missing due to assembly incompleteness and those that exhibit real sequence

991 divergence. Note that human and mouse are not shown here because both genomes were used
992 to define ultraconserved elements²⁶. (e) Our strategy to annotate coding genes combining
993 various types of gene evidences. (f) Comparison of the completeness of gene annotations, using
994 4101 BUSCO genes, and the number of annotated genes. (f) Bar charts compare genome sizes
995 and the proportion that consist of major transposon classes. (g) Fraction of the genome that
996 consists of recent transposon insertions, defined as transposons that diverged less than 6.6%
997 from their consensus sequence.

998

999

1000

1001

1002

1003

1004

1005

1006

1007

1008

1009

1010

1011

1012

1013

1014

1015

1016

1017

1018

1019

1020

1021

1022

1023

1024

1025

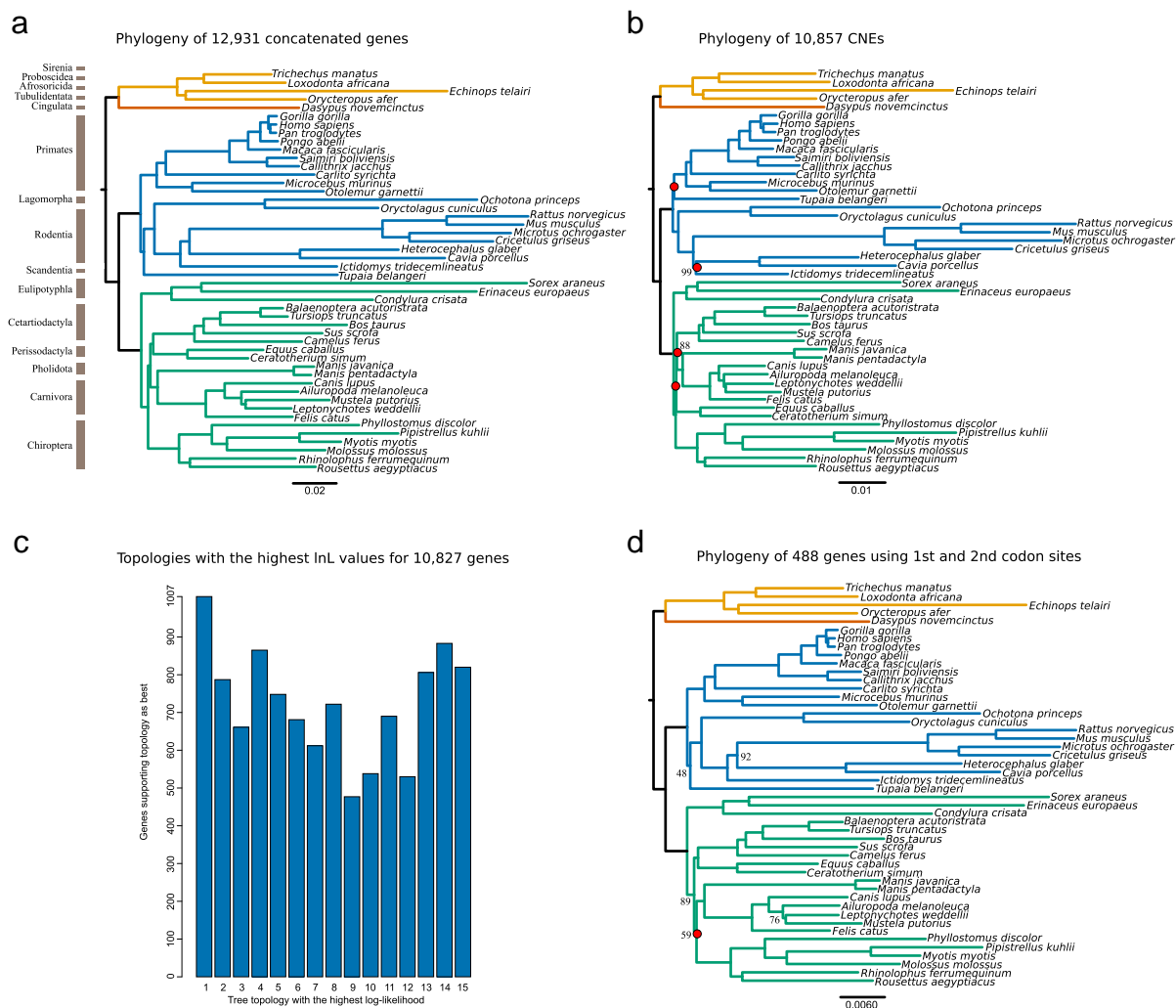
1026

1027

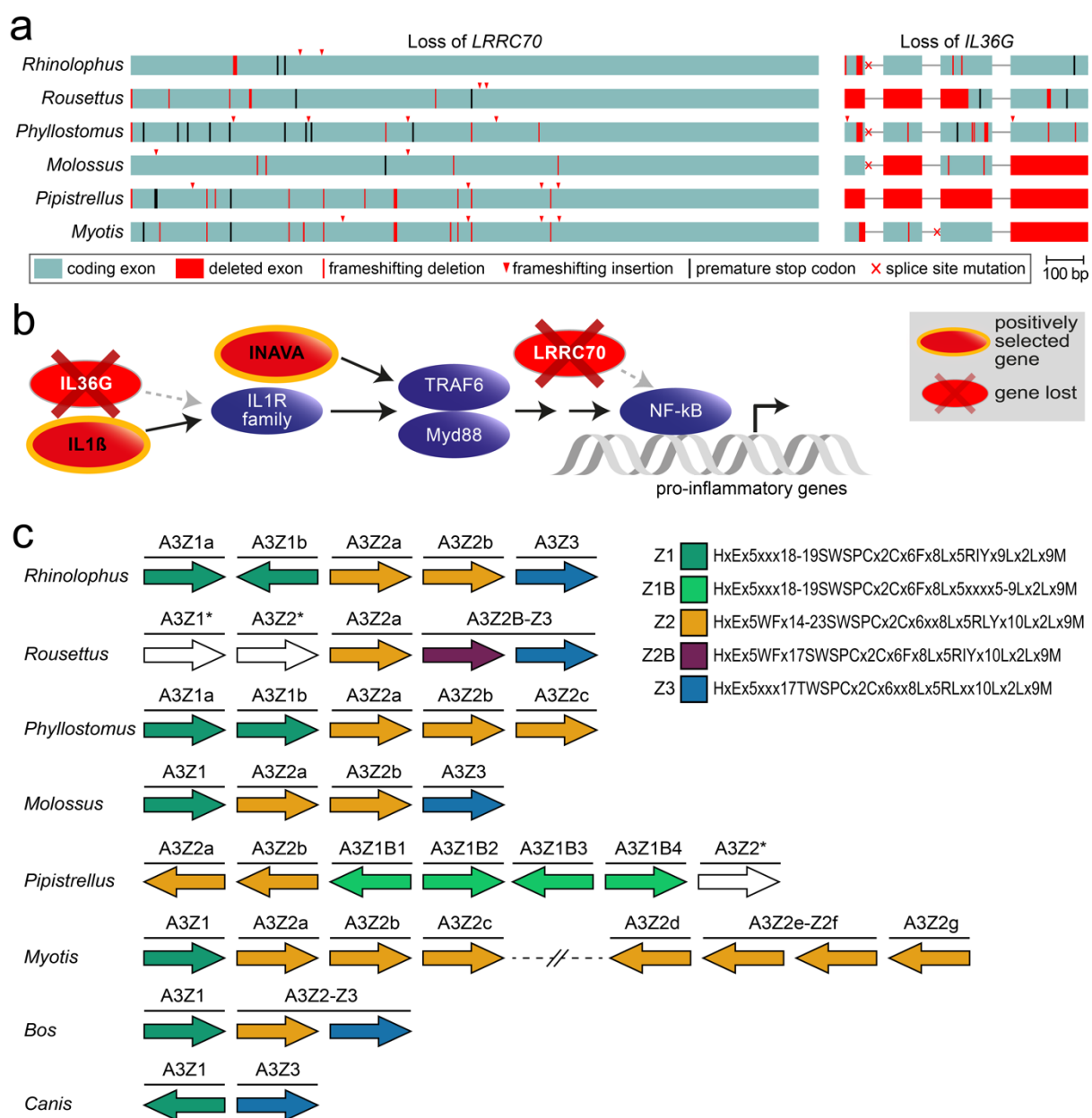
1028

1029

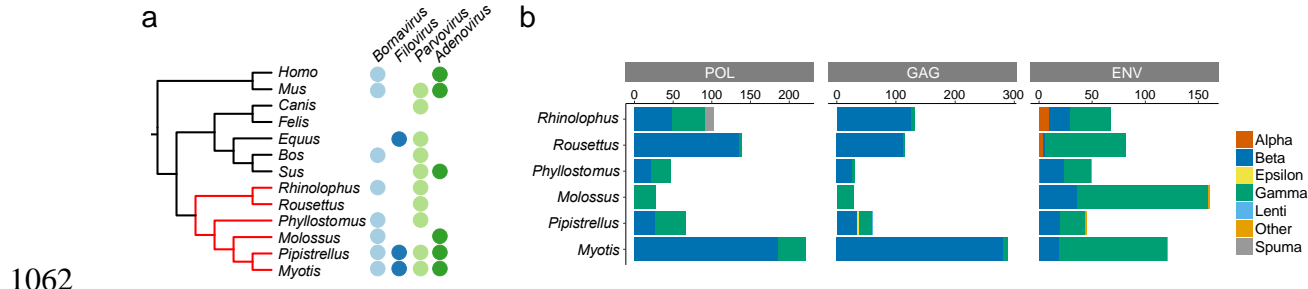
1030

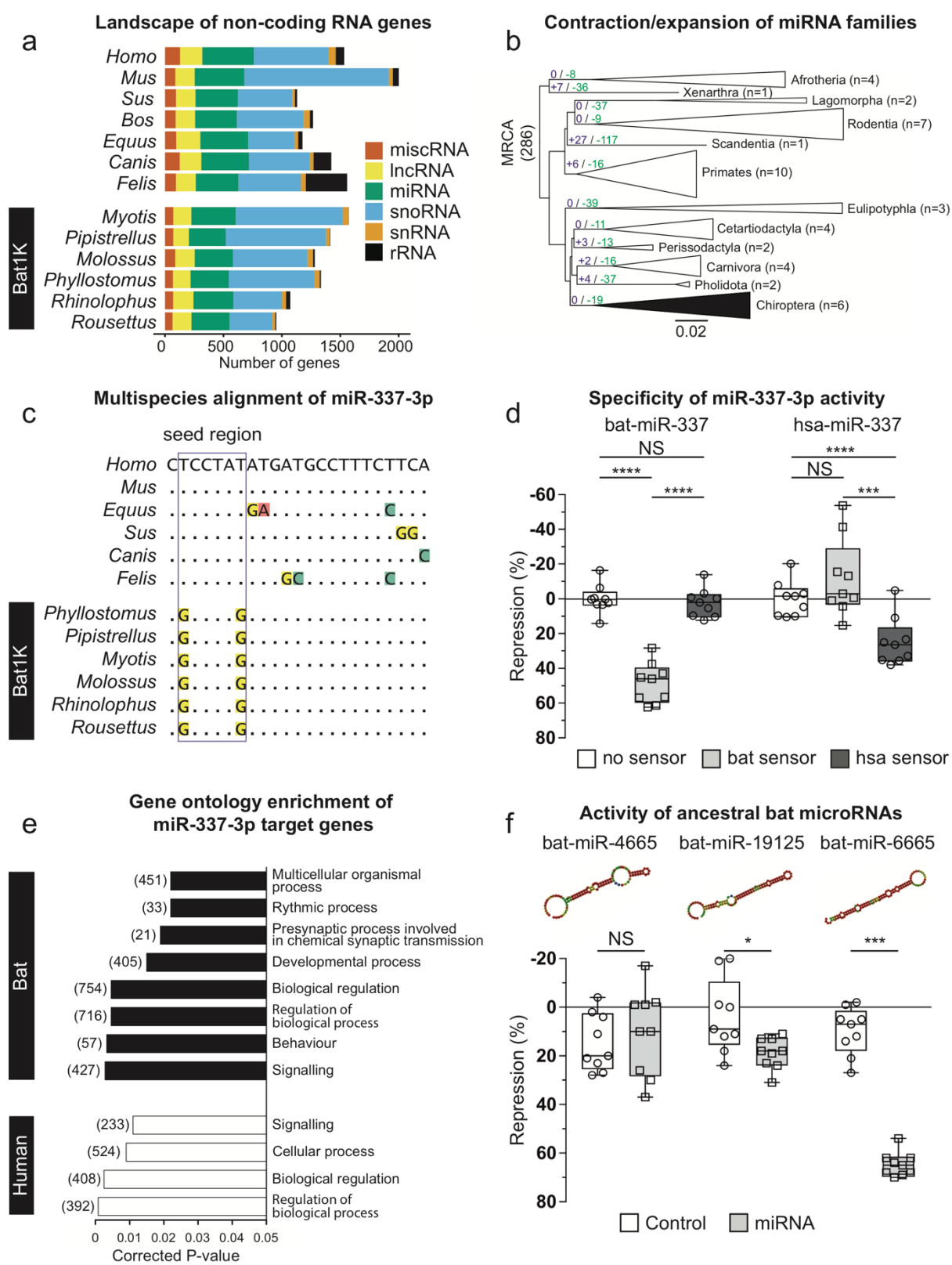


1031
1032
1033 **Figure 2: Phylogenetic analysis of Laurasiatheria.** (a) We inferred a mammalian phylogram
1034 using a supermatrix of 12,931 concatenated genes and the maximum likelihood method of tree
1035 reconstruction (topology 1, Fig. S6). (b) A total of 10,857 conserved non-coding elements
1036 (CNEs) were used to determine a mammalian phylogeny using non-coding regions (topology
1037 2, Fig. S6). Bootstrap support values less than 100 are displayed, with internal nodes that differ
1038 to the protein-coding supermatrix highlighted in red. (c) All gene alignments were fit to the 15
1039 laurasiatherian topologies (Fig. S6) explored to determine which tree had the highest likelihood
1040 score for each gene. The number of genes supporting each topology are displayed. (d) A
1041 supermatrix consisting of 1st and 2nd codon sites from 448 genes that are evolving under
1042 homogenous conditions, thus considered optimal ‘fit’ for phylogenetic analysis, was used to
1043 infer a phylogeny using maximum likelihood (topology 13 Feig. S6). Bootstrap support values
1044 less than 100 are displayed, with internal nodes that differ to the protein-coding supermatrix
1045 phylogeny highlighted in red.
1046



1047
1048
1049 **Figure 3: Genome-wide screens highlight changes in genes potentially involved in bat's
1050 unique immunity.** (a) Inactivation of the immune genes *LRRC70* and *IL36G*. Boxes represent
1051 coding exons proportional to their size, overlaid with gene-inactivating mutations present in
1052 the six bats. (b) Diagram showing the canonical NF-κB signalling pathway (purple) and
1053 interacting proteins which have experienced positive selection or have been lost in bats. (c)
1054 Expansion of the *APOBEC3* gene locus in bats. Each arrow represents a cytidine deaminase
1055 domain, coloured by domain subtypes as defined by given motifs, with likely pseudogenes are
1056 in white. Genes containing multiple deaminase domains are shown as a single bar over more
1057 than one domain. A transposition event in *Myotis* has created two *APOBEC3* loci on different
1058 chromosomes, indicated by the broken line in this species. Cow and dog are shown as two
1059 Laurasiatheria outgroups, where cow also represents the likely, mammalian ancestral state.
1060
1061





1071

1072

1073

1074

1075

1076

1077

Figure 5: The evolution of non-coding RNA genes in bats (a) The number of non-coding RNA genes annotated in six bat genomes and 7 reference mammalian genomes. (b) miRNA family expansion and contraction analyses in 48 mammalian genomes. The numbers highlighted on the branches designate the number of miRNA families expanded (purple, +) and contracted (green, -) at the order level. n indicates the number of species in each order used in the analysis. (c) The alignment of the mature miR-337-3p sequences across six bats and six

1078 reference species (miR-337-3p could not be found in *Bos taurus* genome). The box indicates
1079 the seed region of mature miR-337-3p, which is conserved across mammals, but divergent in
1080 bats. (d) Specificity of human (hsa) and bat miR-337-3p activity was shown using species
1081 specific sensors in luciferase reporter assays (n=9 per experiment; see supplementary methods
1082 section 5.4). Significance was calculated using two-way ANOVA test, followed by post-hoc
1083 Tukey calculation. Statistical significance is indicated as: ***p<0.001; ****p<0.0001. (e)
1084 Gene ontology enrichment (via DAVID) of targets predicted for human and bat miR-337-3p
1085 (f) Validation of the activity of ancestral bat miRNAs, absent in the other mammalian genomes.
1086 The predicted secondary structures for each novel miRNA are displayed. For each miRNA, the
1087 sensor was tested against a control unrelated miRNA that was not predicted to bind to the
1088 sensor (left) and the cognate miRNA (right) in luciferase reporter assays (n=9 per experiment;
1089 see supplementary methods section 5.4). Significance for each independent control-miRNA
1090 pair was calculated using pairwise t tests. Statistical significance is indicated as: *p<0.05;
1091 ***p<0.001. Box plots extend from the 25th to 75th percentiles, the central line represents the
1092 median value, and whiskers are drawn using the function “min to max” in GraphPad Prism7
1093 (GraphPad Software, La Jolla California USA, <http://www.graphpad.com>) and go down to the
1094 smallest value and up to the largest.
1095